Effects of the Geometry of the Rotor Slots on the Mechanical Vibration of Three-phase Induction Motors

P.PAO-LA-OR[*Ψ], S.PEAIYOUNG[**], T.KULWORAWANICHPONG[*], and S.SUJITJORN[*]
[*]School of Electrical Engineering, Institute of Engineering,
Suranaree University of Technology, Nakhon Ratchasima, 30000, THAILAND
[**]RTAF Academy, Air Education and Training Command,
Bangkok, 10220, THAILAND

Abstract: - This paper presents the development of mathematical models and simulations of magnetic field, and mechanical vibration in a three-phase squirrel-cage induction motor. Its aim is to compare the vibration magnitude when the motor possesses different geometrical rotor-slot shapes. The cross sectional areas of two typical semi-closed slot shapes (rectangular and round shapes) are kept equally constant according to the IEEE standard. Under an assumption of sinusoidal motor excitation, the simulation works employ the finite element method (FEM) and the Newton-Raphson method to solve time varying nonlinear equations. The numerical solutions obtained indicate the electromagnetic force distribution over the motor cross sectional area. Such forces cause mechanical vibration in the motor. To evaluate this vibration, the displacement of stator inner perimeters was observed carefully. As a result, the round rotor slot gives 4.8% less vibration than the rectangular rotor slot does.

Key-Words: - Mechanical Vibration, Electromagnetic Force, Computer Simulation, Finite Element Method, Induction Motors, Rotor Slots

1 Introduction

Mechanical vibration in induction motors has a long history. In previous works, the study of an induction motor considered resultant motor vibration. The works during 1990-1993 [1,2] considered vibration caused by rotor eccentricity, and supply harmonic produced by an inverter source. The work [3] studied the effects of rotor slot skewness on motor vibration. From 1997 till present, the number of stator and rotor slots has been carefully designed to reduce motor vibration [4,5]. The study of the shapes of rotor slots that influence the motor vibration has not been considered before. This is an important issue addressed by this paper. By our approach, comparison studies of rotor slot shapes affecting motor vibration according to two IEEE standard shapes have been accomplished [6].

This paper illustrates a numerical approach to magnetic field modelling of a squirrel-cage induction motor fed by a sinusoidal source. The two-dimensional nonlinear time-stepping finite element method (FEM) is used for electromagnetic field approximation in the motor operating with full-load steady-state revolution. The computed electromagnetic forces are used as the external forces applied to the motor to cause vibration. The approaches of vibration analysis are FEM. The effects of the rotor slot shapes on vibration are also investigated.

2 Modelling for Computational Electromagnetic and Mechanic

In magnetic field calculation, the magnetic vector potential **A** carries a bundle of information consisting of flux density **B**, and induced magnetic forces **F**. For convenience, some assumptions are made as follows: the magnetic field presents in the cross-sectional (*x,y*) plane; the magnetic materials of the cores are nonlinearly isotropic. Hence, Eq. (1) describes the temporal and spatial variations of **A** [7].

$$\frac{\partial}{\partial x}\left(\nu\frac{\partial \mathbf{A}}{\partial x}\right)+\frac{\partial}{\partial y}\left(\nu\frac{\partial \mathbf{A}}{\partial y}\right)-\mathrm{s}\sigma\left(\frac{\partial \mathbf{A}}{\partial t}\right)+\mathbf{J}_0=0 \qquad (1)$$

where ν is the reluctivity of the material, σ is the conductivity of the rotor conducting media, s is the motor slip, and $\mathbf{J_0}$ is the applied current density.

Our works [8,9] have utilized the finite element method for solving the equation (1). We adopted the Galerkin weighted residual method to derive the element equation on the basis of the Maxwell's equations. Resulting from equation (1) with the

Galerkin weighted residual method applied [10], we arrive at the following expression

$$[M]\{\dot{A}\}+[K]\{A\}=\{F\} \tag{2}$$

,where

$$[M]=\frac{s\sigma\Delta_e}{12}\begin{bmatrix}2&1&1\\1&2&1\\1&1&2\end{bmatrix}$$

$$[K]=\frac{v}{4\Delta_e}\begin{bmatrix}b_ib_i+c_ic_i & b_ib_j+c_ic_j & b_ib_k+c_ic_k\\ & b_jb_j+c_jc_j & b_jb_k+c_jc_k\\ Sym & & b_kb_k+c_kc_k\end{bmatrix}$$

$$\{F\}=\frac{J_0\Delta_e}{3}\begin{bmatrix}1\\1\\1\end{bmatrix}$$

,where Δ_e is the area of the triangular element, which is

$$\Delta_e=\frac{1}{2}\begin{vmatrix}1&x_i&y_i\\1&x_j&y_j\\1&x_k&y_k\end{vmatrix}$$

$$a_i=x_jy_k-x_ky_j,\quad b_i=y_j-y_k,\quad c_i=x_k-x_j$$
$$a_j=x_ky_i-x_iy_k,\quad b_j=y_k-y_i,\quad c_j=x_i-x_k$$
$$a_k=x_iy_j-x_jy_i,\quad b_k=y_i-y_j,\quad c_k=x_j-x_i$$

The equation (2) describes the magnetic vector potential as a space-time function.

To simulate the motor movement, we need to discretize equation (2). We use the backward difference method for the discretization because of its good convergent property. Hence, the time derivatives of the magnetic vector potential can be expressed by

$$\{\dot{A}\}^{t+\Delta t}=\frac{\{A\}^{t+\Delta t}-\{A\}^{t}}{\Delta t} \tag{3}$$

The discrete form of equation (2) at time $t+\Delta t$ is

$$[M]\{\dot{A}\}^{t+\Delta t}+[K]\{A\}^{t+\Delta t}=\{F\}^{t+\Delta t} \tag{4}$$

Inserting equation (3) into equation (4), one could obtain

$$\left(\frac{1}{\Delta t}[M]+[K]\right)\{A\}^{t+\Delta t}=\frac{1}{\Delta t}[M]\{A\}^{t}+\{F\}^{t+\Delta t} \tag{5}$$

To solve equation (5) requires an efficient iterative method of solving nonlinear time-stepping equations. We apply the N-R method to solve the equations. Additionally, our approach employs the BCG method as its internal structure to solve linearized equations. Regarding to the approach, the matrix form of the N-R equation governing the element can be found as equation (6), where the left-most matrix is Jacobian

$$\begin{bmatrix}\frac{\partial G}{\partial A_i^{t+\Delta t}} & \frac{\partial G}{\partial A_j^{t+\Delta t}} & \frac{\partial G}{\partial A_k^{t+\Delta t}}\\ \frac{\partial H}{\partial A_i^{t+\Delta t}} & \frac{\partial H}{\partial A_j^{t+\Delta t}} & \frac{\partial H}{\partial A_k^{t+\Delta t}}\\ \frac{\partial I}{\partial A_i^{t+\Delta t}} & \frac{\partial I}{\partial A_j^{t+\Delta t}} & \frac{\partial I}{\partial A_k^{t+\Delta t}}\end{bmatrix}\begin{bmatrix}\Delta A_i^{t+\Delta t}\\ \Delta A_j^{t+\Delta t}\\ \Delta A_k^{t+\Delta t}\end{bmatrix}=-\begin{bmatrix}G\\H\\I\end{bmatrix} \tag{6}$$

,in which G, H and I represent the first, second and third row equations embedded in equation (5), respectively.

Figure 1 shows the proposed semi-closed rotor slot shapes which have equal cross-sectional areas. The cross-sections of the motors are discretized into minute triangular elements. Figure 2 shows some parts of the discretized cross-sections. The entire cross-section of a motor for each slot shape contains 5,224 elements and 2,688 nodes.

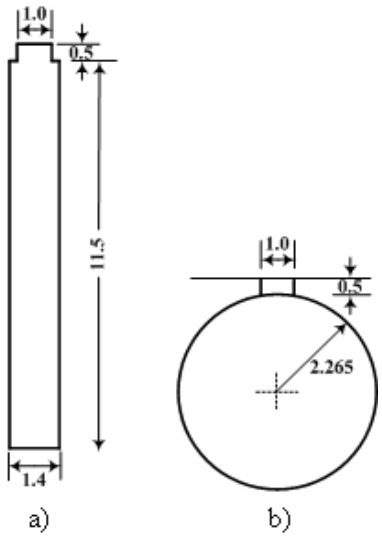

Fig. 1. Dimensions (in mm) of rotor slot shapes: a) rectangular rotor slot, b) round rotor slot

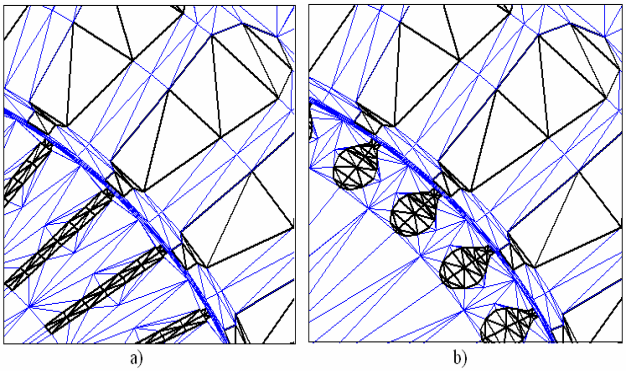

Fig. 2. Discretized cross-section of an induction motor: a) rectangular rotor slot, b) round rotor slot

The finite element approach is also utilized to calculate the motor's vibration. The motion can be described by equation (7), in which [*M*], [*C*], and [*K*] are the mass, damping, and stiffness matrices, respectively. {*F*} represents the external force vector. For our computational vibration, the stator core and the motor frame are considered. It is assumed that the force acting on the center of each stator tooth could be transmitted through to the motor frame [11].

$$[M]\{\ddot{d}\}+[C]\{\dot{d}\}+[K]\{d\}=\{F\} \quad (7)$$

The force applied to the motor is the computed magnetic force at the center of each stator tooth. In addition, the motors are considered to have thin-plate cross sections [12].

3 Results and Discussion

The machine considered by this study is a three-phase, four-pole, Y-connected, 5-hp squirrel cage induction motor with a double layer winding of 7/9 pitch coil. The motor possesses 36 stator slots and 44 un-skewed rotor slots. The sinusoidal source provides a 380-V, 50-Hz at full load (slip, s =0.03). The computation of flux lines and electromagnetic forces was conducted using an FEM solver developed in C by the authors. Numerical results of the magnetic vector potential for each case are illustrated as shown in figure 3. Figure 3 illustrates the flux line distributions through the motor cross-sections corresponding to the rotor slot shapes. As can be seen, the rectangular rotor slot produces more linkage flux flowing into the slot than that of the round rotor slot. The curl of the magnetic vector potential **A** is magnetic flux density **B** (**B** = **∇**×**A**). Maxwell's stress equations were used to determine the distribution of the magnetic forces across the air gap. Surface plots in figure 4 disclose the space-time distributions of the radial forces as our computational results according to the rotor slot shapes. The rectangular rotor slot gives slightly higher radial forces, which cause motor vibration, than the round type does.

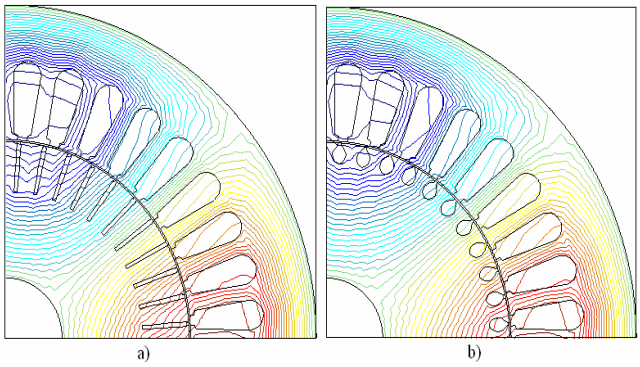

Fig. 3. Flux line distribution: a) rectangular rotor slot, b) round rotor slot

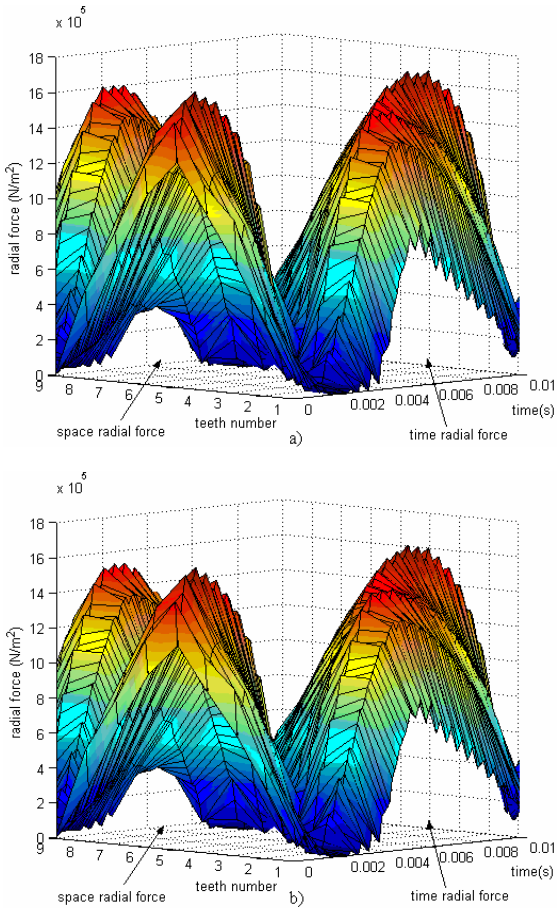

Fig. 4. Space-time distribution of radial forces: a) rectangular rotor slot, b) round rotor slot

Our FEM solver developed in C has been used to solve the motion equation to obtain the vibration solutions. The FEM solver provides solutions

disclosing the distortions of the stator inner perimeter as shown in figures 5 and 6, for the rectangular and the round rotor slots, respectively. The solid lines in these figures represent the perimeter in normal situation. The dashed lines show the instantaneous displacement or distortion magnified by 10^9 times. The average displacements in one revolution are 6.1963×10^{-8} and 5.8989×10^{-8} mm corresponding to the rectangular slot and the round slot, respectively. In the mechanical vibration point of view, the round shape gives 4.8% less vibration than the rectangular one does due to the shallowness of the circle slot. Therefore, there are less magnetic flux lines flowing into the slot in this case, to cause less vibration, compared with the deeper slot of the rectangular type.

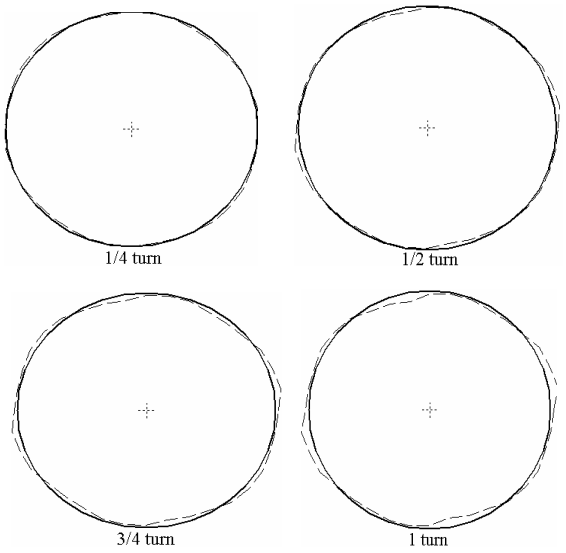

Fig. 5. Distortion of the stator inner perimeter corresponding to the rectangular rotor slot

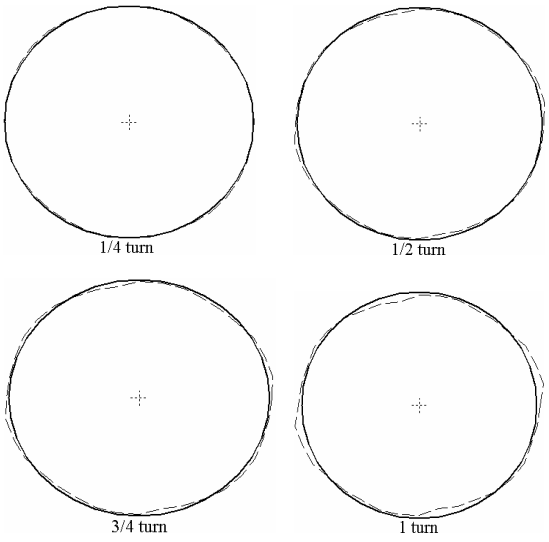

Fig. 6. Distortion of the stator inner perimeter corresponding to the round rotor slot

4 Conclusions

This paper presents the mathematical description and the graphical interpretation for mechanical vibration of induction motors resulting from induced electromagnetic forces. When the IEEE standard rotor slot shapes of equal slot areas, i.e. i) rectangular shape and ii) round shape, are challenged by observing the mechanical vibration around the stator inner perimeter, the round case gives less vibration of 4.8% than the rectangular case does. We can conclude that when the mechanical vibration is taken into account in the rotor slot design, the round shape is preferable to give less vibration than the rectangular one, at least by the results from our comprehensive studies. However, for completion of motor's rotor design, other factors, such as torque-speed curves, harmonic current drawn from supply, etc., are also vital and should also be considered during the design phase.

References:

[1] R.J.M. Belmans, D. Verdyck, W. Geysen, R.D. Findlay, Electro-mechanical analysis of the audible noise of an inverter-fed squirrel-cage induction motor, *IEEE Transactions on Industry Applications,* Vol.27, No.3, 1991, pp. 539-544.

[2] W.R. Finley, Noise in induction motors-causes and treatments, *IEEE Transactions on Industry Applications,* Vol.27, No.6, 1991, pp. 1204-1213.

[3] D.G. Dorrell, Calculation of unbalanced magnetic pull in small cage induction motors with skewed rotors and dynamic rotor eccentricity, *IEEE Transactions on Energy Conversion,* Vol.11, No.3, 1996, pp. 483-488.

[4] T. Kobayashi, F. Tajima, M. Ito, S. Shibukawa, Effects of slot combination on acoustic noise from induction motors, *IEEE Transactions on Magnetics,* Vol.33, No.2, 1997, pp. 2101-2104.

[5] B.T. Kim, B.I. Kwon, S.C.Park, Reduction of electromagnetic force harmonics in asynchronous traction motor by adapting the rotor slot number, *IEEE Transactions on Magnetics,* Vol.35, No.5, 1999, pp. 3742-3744.

[6] I. Boldea, S.A. Naser, *The induction machine handbook*, Florida, USA, 2002.

[7] M.E. Nagwa, R.E. Anthony, E.D. Graham, Detection of broken bars in the cage rotor on an induction machine, *IEEE Transactions on Industry Applications,* Vol.28, No.1, 1992, pp. 165-171.

[8] P. Pao-la-or, S. Peaiyoung, T. Kulworawanichpong, S. Sujitjorn, Modelling

and simulation for magnetic flux distribution in induction motors, *Proc. the 24th IASTED International Conference on Modelling, Identification, and Control (MIC 2005),* Austria, 2005, pp. 339-344.

[9] P. Pao-la-or, T. Kulworawanichpong, S. Sujitjorn, S. Peaiyoung, Distributions of Flux and Electromagnetic Force in Induction Motors: A Finite Element Approach, *WSEAS Transactions on Systems*, Vol. 5, No. 3, 2006, pp. 617-624.

[10] T.W. Preston, A.B.J. Reece, P.S. Sangha, Induction motor analysis by time-stepping techniques, *IEEE Transactions on Magnetics*, Vol.24, No.1, 1988, pp. 471-474.

[11] F. Ishibashi, K. Kamimoto, S. Noda, K. Itomi, Small induction motor noise calculation, *IEEE Transactions on Energy Conversion,* Vol.18, No.3, 2003, pp. 357-361.

[12] J.S. Rao, *Dynamics of plates*, Narosa Publisher, New Delhi, 1999.